Journal of Nuclear Materials 381 (2008) 98–105

Contents lists available at ScienceDirect

Journal of Nuclear Materials

journal homepage: www.elsevier.com/locate/jnucmat

Comparison of 3 MeV C^+ ion-irradiation effects between the nuclear graphites made of pitch and petroleum cokes

Se-Hwan Chi *, Gen-Chan Kim

Nuclear Hydrogen Development and Demonstration Project, Korea Atomic Energy Research Institute, P.O. Box 105, Yuseong, Daejeon 305-600, Republic of Korea

ARTICLE INFO

PACS:
81.05.Uw
81.40.−z
81.40.Wx
81.65.Mg

ABSTRACT

Three million electron volt C^+ irradiation effects on the microstructure (crystallinity, crystal size), mechanical properties (hardness, Young's modulus) and oxidation of IG-110 (petroleum coke) and IG-430 (pitch coke) nuclear graphites were compared based on the materials characteristics (degree of graphitization (DOG), density, porosity, type of coke, Mrozowski cracks) of the grades and the ion-irradiation conditions. The specimens were irradiated up to ~19 dpa at room temperature. Differences in the as-received microstructure were examined by Raman spectroscopy, X-ray diffraction (XRD), optical microscope (OM) and transmission electron microscope (TEM). The ion-induced changes in the microstructure, mechanical properties and oxidation characteristics were examined by the Raman spectroscopy, microhardness and Young's modulus measurements, and scanning electron microscope (SEM). Results of the as-received microstructure condition show that the DOG of the grades appeared the same at 0.837. The size of Mrozowski cracks appeared larger in the IG-110 of the higher open and total porosity than the IG-430. After an irradiation, the changes in the crystallinity and the crystallite size, both estimated by the Raman spectrum parameters, appeared large for the IG-430 and the IG-110, respectively. The hardness had increased after an irradiation, but, the hardness increasing behaviors were reversed at around 14 dpa. Thus, the IG-430 showed a higher increase before 14 dpa, but the IG-110 showed a higher increase after 14 dpa. No-clear differences in the increase of the Young's modulus were observed between the grades mainly due to a scattering in the measurements results. The IG-110 showed a higher oxidation rate than the IG-430 both before and after an irradiation. Besides the density and porosity, a possible contribution of the well-developed Mrozowski cracks in the IG-110 was noted for the observation. All the comparisons show that, even when the differences between the grades are not large, the results of the oxidation and hardness test show a higher irradiation sensitivity for the IG-110. The similar irradiation sensitivities between the grades were attributed to the same degree of graphitization (DOG) of the grades.

1. Introduction

Recently, with the development of a very high temperature gas-cooled reactor (VHTR) within the Generation-IV (GIV) next generation nuclear energy system development road map, a number of studies on nuclear graphite are being planned, and some are being performed in those countries participating in the GIV VHTR project management boards (PMB)-Materials. The backgrounds for the graphite studies are described well in the work package plan for the graphite technology development area. Thus, several new grades of nuclear graphite have been developed since the graphites developed in the 1970s and 80s for advanced gas-cooled reactor applications are no longer in production. Consequently, codes and standard, material properties and behavior data must be developed to support the design and construction of structures associated with new Generation-IV reactor concepts [1,2].

Of those various R&D topics, studies on the selection of the grades, qualification of the selected grades, and preparation of a database for the design of VHTR have been the major subjects of common interest. Especially, studies on radiation effects have been recognized as important not only for the selection but also for the qualification of the candidate grades. It is well known, however, that the development of neutron irradiation data on graphite is difficult, expensive, and time consuming. In this case, the use of an ion-accelerator can be a useful tool for a neutron radiation damage simulation by a charged-particle irradiation, and to compare the irradiation effects of the candidate grades in the same irradiation conditions for the purpose of a selection [3].

On the other hand, regarding the selection of the grades, since the virgin and irradiated graphite properties depend strongly on the raw materials and manufacturing processes, information on the effects of the differences in the raw materials on an irradiation-induced

* Corresponding author.
E-mail address: shchi@kaeri.re.kr (S.-H. Chi).

0022-3115/$ - see front matter © 2008 Elsevier B.V. All rights reserved.
doi:10.1016/j.jnucmat.2008.08.001

property change are also important during the selection process of the grades. Currently, most of the commercially available nuclear graphite is made of coke (~75%) and a binder (~25%), and only two types of coke, i.e., pitch or petroleum, are being used for manufacturing the artificial nuclear graphite for a VHTR [4].

In the present study, based on the two discussions above, nuclear graphite specimens made of pitch coke or petroleum coke were irradiated to 3 MeV C^+ ion by using an accelerator, and comparisons were made between the grades to provide the basic information necessary for an understanding of the radiation effects on nuclear graphite and for the selection of the nuclear graphite for the VHTR.

2. Experimental procedure

2.1. Materials and specimen preparation

The materials used in the present study are IG-110 and IG-430 isotropic nuclear graphites manufactured by Toyo Tanso. From two nuclear graphite blocks (size: 300 × 300 × 200 mm each) of IG-110 (petroleum coke) and IG-430 (pitch coke), specimens with a size of 10 × 10 × 2 (mm^3) were prepared by a mechanical polishing up to 0.05 μm Al_2O_3 and followed by a cloth polishing and ultrasonic cleaning for the irradiation and the as-received baseline property measurements: i.e., hardness, Young's modulus, Raman spectrum, and the oxidation rate. Table 1 compares some of the physical and mechanical properties reported in the manufacturer's materials test sheet.

2.2. Optical microscopy, TEM, XRD, porosimetry and ion-irradiation

After a fine polishing (0.05 μm Al_2O_3 and followed by a cloth polishing), the specimens were ultrasonic cleaned, and a polarized light was used for the optical microscopy (OM). TEM was performed to investigate the possible differences in the crystal structure such as the Mrozowski cracks. For TEM, after preparing 3 mm∅ disks (thickness ≈0.5 mm) by using an ultrasonic disk cutter and a polishing up to No. 2000 SiC paper, all the specimens were dimpled ($t \leqslant 10$ μm) using a 30 g load and 1 μm paste, and ion-milled (Ar, 3 KeV–14 μA).

To estimate the degree of graphitization (DOG: $\bar{g}$) from the lattice parameter **c**, XRD measurements with a Cu Kα radiation were conducted by referring to the Japanese procedure for measurements of the lattice parameters and the crystallites sizes of carbon materials by an X-ray diffraction [5]. The DOG was determined from the following Eq. (1),

$$\bar{g} = \frac{[3.440 - d(002)]}{[3.440 - 3.354]} \tag{1}$$

Table 1
Comparison of some of the physical and mechanical properties of IG-110 and IG-430 nuclear graphite (manufacturer data sheet)

Grade	IG-110	IG-430
Coke	Petroleum	Coal-tar
Grain size, mm	0.02	0.01
Apparent density, g/cm^3	1.77	1.82
Anisotropy ratio	1.10	1.09
Ash content, ppm	<10	<10
Impurity, ppm	0.001–0.1	0.001–0.1
Young's modulus (*E*), GPa	9.7	10.6
Tensile strength, MPa	27.2	37.8
Compressive strength, MPa	79.0	96.0
Thermal conductivity, W/m	129–140	138–147
Coefficient of thermal expansion (CTE), (10^{-6}/K) RT-400 °C	4.2(Z) 3.8(T)	4.7(Z) 4.3(T)

T: perpendicular to axial direction of the block.
Z: parallel to axial direction of block.

where $d(002) = c/2 = 3.354$ Å for $\bar{g} = 1$ and $d(002) = 3.44$ Å for $\bar{g} = 0$ [6].

To examine the effects of a porosity on the oxidation and the irradiation sensitivity of the grades before and after an irradiation, the total and open porosity were measured based on the apparent and the pycnometric density. The pycnometric density was determined by using the helium gas pycnometer (model: AccuPyc 1330). The total porosity (ε) and closed porosity (ε_c) were determined based on the apparent density (d_V) and the pycnometric density (d_P) as follows:

$$\varepsilon = \left[1 - \frac{d_V}{2.25}\right] \times 100 \tag{2}$$

$$\varepsilon_C = \left[1 - \frac{d_P}{2.25}\right] \times 100 \tag{3}$$

where the value 2.25 g/cm^3 is the density of a graphite single crystal.

The open porosity ε_0 was determined as a difference between that of the total porosity and the closed porosity.

Specimens prepared for an ion-irradiation were irradiated to the peak dose of ~19 dpa by 3 MeV C^+ ions of a 1 μA beam current by using a Tandem Vande-Graff accelerator at room temperature. The range of ions calculated by TRIM 98 was 3.2 μm (E_d = 25 eV).

2.3. Mechanical property measurement: hardness and Young's modulus

Dynamic ultra-microhardness tester (model: Shimadzu DUH-200) was used for a measurement of the hardness (*H*) and Young's modulus. The DUH-200 tester is a very effective tool to trace microhardness changes at a depth of a few microns as appeared in the present ion-irradiated specimen. The tester enables us to measure the change of a load (0.01–200 gf) in depth (0–10 μm) continuously. The hardness (*H*) was determined as $H = P/A$, where: *P* – the maximal load, *A* – projected area of the impression [7]. For the standard Vicker's pyramid, $A = 24.5h_C^2$, where, h_C is the penetration depth of a pyramid. However, in a real case, since the pyramidal indenter has non-ideal form, a specific calibration experiment was performed to evaluate the projected area accurately [8,9]. The stressed zone size during the test was estimated to be about 3.5 times that of the penetration depth of the indenter [10]. Thus, it is thought that the indentation load starts to increase when the indentation depth reaches about 30% of the depth at the damage peak. In the case of a 3.2 μm peak damage depth, the damage peak starts to affect the indentation load at the penetration depth of 0.9–1.0 μm. If irradiated, this penetration depth decreases by an interaction of the stress fields due to the indentation load and the formation of an ion-damaged volume. Actually, in the present experimental condition, the peak indentation loads for the ion-irradiated specimens appeared at about ⩽0.5 μm of an indentation depth [9].

For the Young's modulus determination, relationships between the unloading compliance and Young's modulus were used [7,11]. The effective elastic modulus was calculated by the formula: $E = 0.179\ (S/h_C)$, where *S* is the slope of the unloading curve and h_C is the penetration depth of pyramid. The dose effects on the hardness and elastic modulus were evaluated for the 1 gf test load. More details of the experimental features are described elsewhere [9].

2.4. Raman spectroscopy

The application of a Raman spectroscopy especially for the characterization of an ion-irradiated graphite microstructure

should be useful since the penetration depth of a Raman laser into the graphite is 80–100 nm [12] and the formation of an ion-induced defected microstructure in graphite is limited to the surface (range peak: ~3.5 μm) for 3 MeV C^+.

Raman spectroscopy was performed to estimate the over all development of the graphite structure in the as-received condition, the evolution of a defected microstructure, i.e., the changes in the crystallinity, due to an irradiation, from the changes in the FWHM of D and G-peaks, and the crystallite size from the intensity ratio of the D and G-peak, i.e., $I_D/I_G \propto 1/L_a$ [13], before and after an irradiation. Here, I_D and I_G are the peak intensity of the D (1355 cm^{-1}) and G-peak (1583 cm^{-1}), respectively, and the L_a is the diameter of the crystallite in a basal plane direction.

The Raman spectrums were recorded by a LabRamHR with a LN2 cooled CCD multichannel detector and performed at room temperature in a conventional backscattering geometry. The spectra were excited with the 514.5 nm line of an Ar-ion laser. Laser beam power was 2 mW on the specimen. The Raman parameters of the spectrum peaks were obtained by a Lorentzian fitting [14].

2.5. Oxidation experiment

Oxidation experiments were performed to investigate, firstly, the temperature dependency of the oxidation rate (400–1300 °C), and, secondly, the irradiation effects on the oxidation (750 and 1000 °C, 15–120 min) in the He-2.5% air environment by using a thermogravimeter (TG) (flow rate: 40 CC/min). The differences in the oxidation characteristics as appeared in the oxidized surfaces between the un-irradiated and irradiated IG-110 and IG-430 specimens were investigated by SEM. Detailed condition of the oxidation experiments are reported elsewhere [15].

3. Results

3.1. Comparison of the as-received microstructure (OM, TEM, porosimetry)

Figs. 1 and 2 compare the as-received pore microstructure and the Mrozowski cracks of the grades by OM and TEM, respectively, and Tables 2 and 3 show the results of the porosity and Mrozowski crack size measurements of the grades, respectively. Fig. 1 and Table 2 show that the pore structures of the grades are nearly the same, especially with the same open porosity. However, even when the differences are nearly negligible, Fig. 1 shows that the size and total area of the pores in IG-430 appear somewhat smaller than those of IG-110 corresponding to the results of Table 2, where, even if negligible, the density of the IG-110 of the higher total and closed porosity is slightly smaller than the IG-430. Fig. 1 shows that both the sizes of the pores of the grades are nearly the size of the coke particles, ~20 μm.

Unlike the porosity by OM, Fig. 2 and Table 3 show large differences in the length and width of the Mrozowski cracks between the grades. Even the exact densities of the cracks are not known, Fig. 2, Tables 3 and 4 imply that the size and density of the Mrozowski cracks should be far larger and higher in the IG-110 than the IG-430. Based on the measurements, a slightly higher oxidation rate in the IG-110 may be expected (see Fig. 5).

The Mrozowski cracks are known to be formed by the anisotropic shrinkage effects. A greater shrinkage perpendicular to the layers than parallel to them which occurs during a calcination is responsible for the mechanism. The extent of shrinkage cracking is known to decrease as the graphitizability of the coke decreases [16].

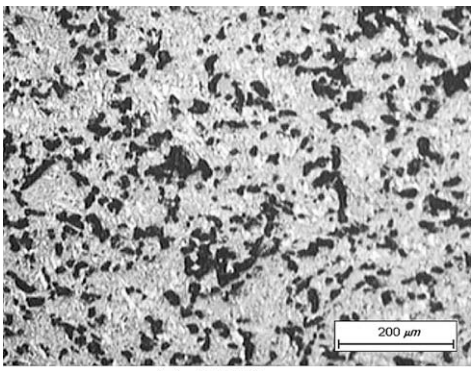

(a) IG-110

(b) IG-430

Fig. 1. As-received optical microstructure of (a) IG-110 and (b) IG-430 graphite.

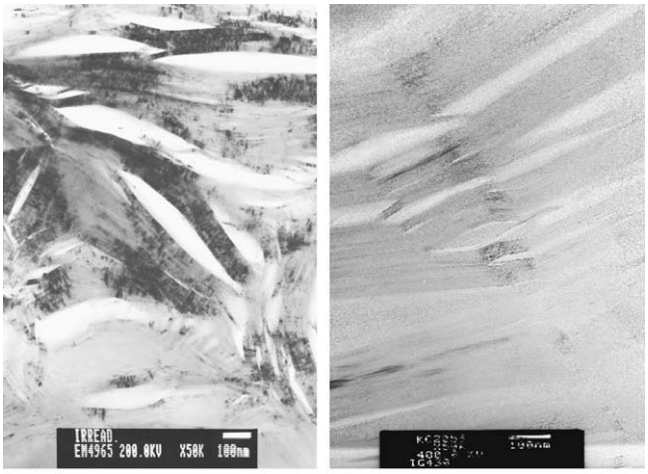

(a) IG-110 (b) IG-430

Fig. 2. TEM microstructure of (a) IG-110 and (b) IG-430 graphites. Different orientations of crystallites can be assumed from the Mrozowski cracks on the (0002) planes. The size of the Mrozowski crack in the IG-110 appears far larger than the IG-430.

Table 2
Determination of the porosity

Characteristics	Graphite	
	IG-110	IG-430
Apparent density (d_V), g/cm^3	1.77	1.82
Pycnometric density (d_P), g/cm^3	2.05	2.10
Total porosity (ε), %	21.33	19.11
Closed porosity (ε_C), %	8.89	6.67
Open porosity (ε_O), %	12.44	12.44

Table 3
Comparison of the width and length of Mrozowski cracks (unit:nm)

Grade	IG-110		IG-430	
	Width	Length	Width	Length
	57.8	450.0	62.1	363.6
	60.9	562.5	62.1	515.1
	71.8	312.5	69.7	484.8
	73.4	593.7	56.0	727.2
	78.1	875.0		
	57.8	450.0		
	176.9	1491.9		
	199.9	2307		
Average	97.1	880.3	62.5	522.7

3.2. Comparison of the degree of graphitization (DOG)

The lattice parameters a and c by XRD, and the degree of graphitization (DOG: $\bar{g}$) by Eq. (1) are summarized in Table 4 for the as-received IG-110 and IG-430.

Table 4 shows that, while the a appeared slightly larger for IG-110, the c, that determines the DOG by Eq. (1), was determined to be the same for both grades at 6.736 Å. This observation may imply a similarity of the graphite manufacturing procedure for both grades, and predicts that the properties related to the DOG will be similar between the grades.

3.3. Comparison of the hardness and Young's modulus

Fig. 3 shows the changes of the hardness (a) and Young's modulus (b) due to a 3 MeV C^+ irradiation at room temperature. Fig. 3 shows that the hardness increase due to an irradiation is higher for the IG-430 up to about 14 dpa, while no-clear differences in the increase of the Young's modulus are observed between the grades mainly due to a scattering of the measurements results.

It is worth noting the reversal of the hardness increase after about 14 dpa, where, the increase in the hardness due to an irradiation (i.e., irradiation sensitivity) became higher for the IG-110 than the IG-430.

3.4. Comparison of the Raman spectrum parameters

Fig. 4(a) shows the Raman spectra of the as-received IG-110 and IG-430, and Table 5 shows the positions and FWHM of the D and G-peaks, and the crystal size of the grades obtained from Fig. 4(a)–(c) show the (FWHM)irr/(FWHM)$_0$ of the D-peak and the (I_D/I_G)irr/$(I_D/I_G)_0$ of IG-110, 5(b), and IG-430 5(c) with the specimen surface dose, respectively. Here, the (FWHM)irr and the (FWHM)$_0$ correspond to the FWHM of D-peak after irradiation (irr) and before irradiation (0) condition, and the (I_D/I_G)irr and $(I_D/I_G)_0$ correspond to the ratio of the intensity of the D-peak to G-peak after irradiation and before an irradiation, respectively.

Table 4
Lattice parameter a, c, and the degree of graphitization (DOG: $\bar{g}$) of the as-received IG-110 and IG-430

	a (Å)	c (Å)	$d(002) = c/2$	$\bar{g}$
IG-110	2.4575	6.736	3.368	0.837
IG-430	2.3606	6.736	3.368	0.837

Both Fig. 4(a) and Table 5 show that the over all as-received material structure of the grades are nearly the same in view of the relationships between the FWHM and the crystallinity [17] even a somewhat large difference is observed in the crystal size (L_a), where, the crystal size of the IG-430 is estimated to be 38% smaller than the IG-110. It is worth noting that the observed similarity between the grades by the Raman spectroscopy is corresponds well to the result of the XRD of the same DOG for both grades, Table 4. It is observed that the higher the crystallinity, the narrower the FWHM of the G-peaks, and the higher the irradiation-induced damage, the wider the FWHM of the D-peak [18,19].

In Figs. 4(b) and (c), from the changes of (FWHM)irr/(FWHM)$_0$ and (I_D/I_G)irr/$(I_D/I_G)_0$ with the dose, the irradiation sensitivity of the grades may be predicted and compared based on the assumed changes in the graphite surface crystallinity (graphite surface bonding microstructure) due to a defect accumulation. Fig. 4(b) and (c) show that the (FWHM)irr/(FWHM)$_0$ of IG-110 and IG-430 are 6.8 and 8.2 at ~0.6 dpa, respectively. From the observation, even when the difference is practically not critical, it is predicted that the changes in the crystallinity due to an irradiation may be slightly higher in IG-430. Here, the changes in the FWHM of the D-peak were recorded based on the observation that, while both the FWHM of the G and D-peaks increase with an irradiation, the increase in the D-peak is relatively larger than that of the G-peak especially in the early stages of an irradiation [18,20,21].

Changes in the crystallite size due to an irradiation, estimated from the ratio of the peak intensity of the D-peak to that of the G-peak, I_D/I_G, show that the crystallite sizes of the IG-110 and IG-

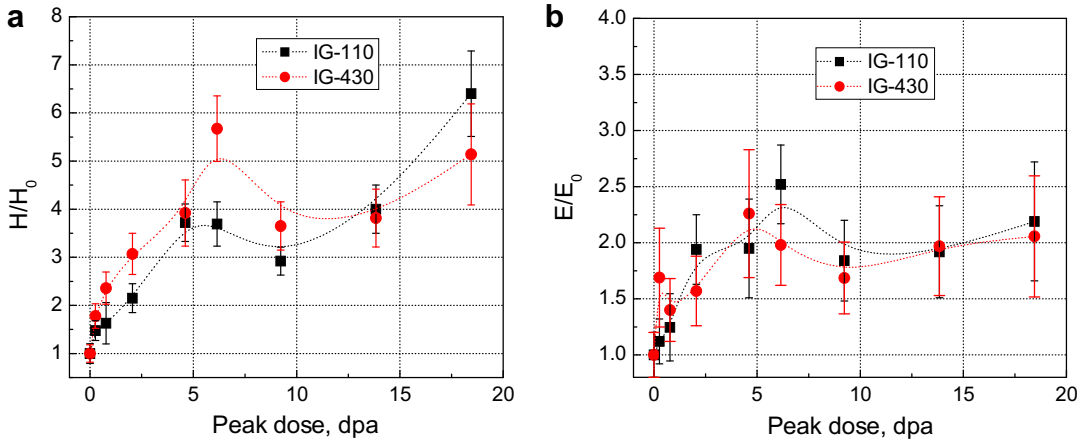

Fig. 3. Comparison of the changes in the hardness (a) and Young's modulus (b) of IG-110 and IG-430 nuclear graphite due to 3 MeV C^+ irradiation. Note that the hardness and Young's modulus value in the figure are normalized with the un-irradiated hardness (H_0) and un-irradiated Young's modulus (E_0), respectively. A comparison of the figures shows that the measurement of the irradiation sensitivity is far higher for the hardness than the Young's modulus.

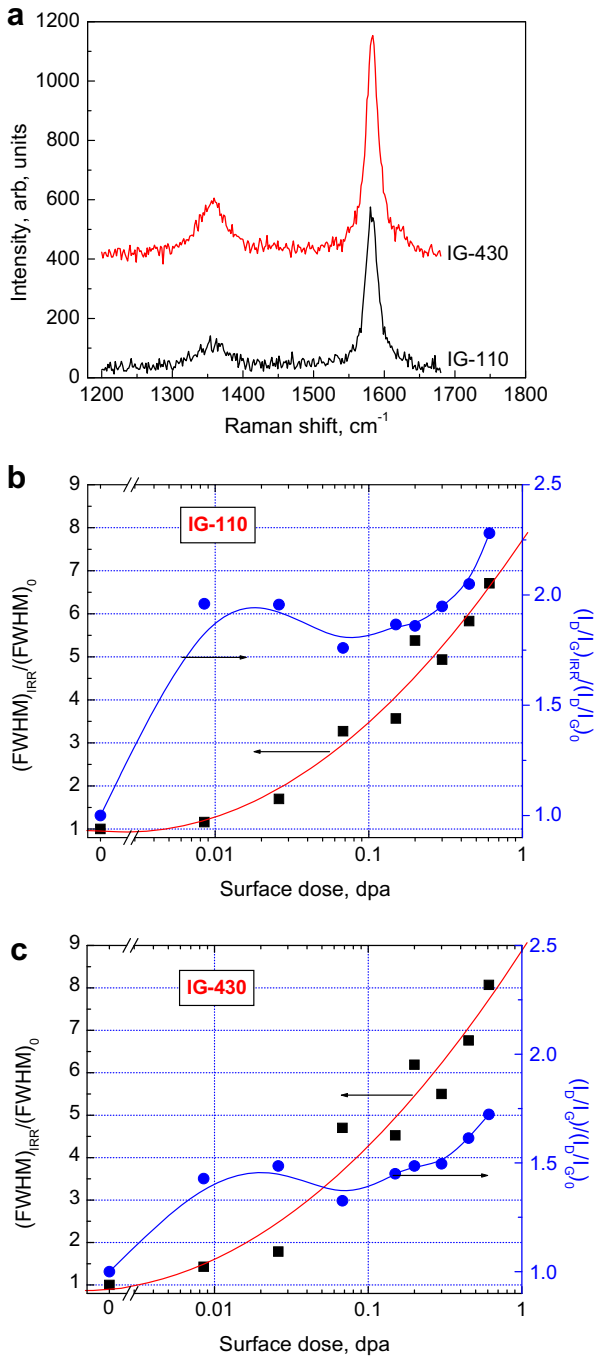

Fig. 4. Comparisons of (a) the as-received Raman spectra between the IG-110 and IG-430, and the changes in the (FWHM)irr/(FWHM)$_0$ of the D-peak, and the (I_D/I_G)irr/$(I_D/I_G)_0$ due to the 3 MeV C^+ ion-irradiation dose for (b) IG-110, and (c) IG-430 grades.

Table 5
Comparison of the Raman shift, FWHM, and the crystallite size (L_a) estimated from the intensity ratio between the D and G-peaks of the as-received IG-110 and IG-430 grades

Grades		Raman shift, cm^{-1}	FWHM, cm^{-1}	Crystal size (L_a), nm
IG-110	D-peak	1356.9	48.9	30.6
	G-peak	1582.2	19.9	
IG-430	D-peak	1356.5	42.7	18.9
	G-peak	1583.1	20.9	

430 were estimated to be decreased by ~1/2.3, i.e., from 30.6 to 13.3 nm, and ~1/1.7, i.e., from 18.9 to 11.1 nm, respectively. It appears that the larger the initial crystallite size, the larger the decrease in a crystallite size resulting in a decreased difference between the grades after an irradiation. Here, it is worth noting the reversed reaction of the crystallinity and crystallite size of the grades when analysed based on the Raman spectroscopy. Thus, for the same dose, while a higher damage to crystallinity occurred in the IG-430, a large decrease in the crystallite size was observed in IG-110.

It is also worth noting that the appearance of the peaks in both grades in the (I_D/I_G)irr/$(I_D/I_G)_0$ curve at ~0.02 dpa may correspond to an amorphization (or disruption of crystallinity) of the graphite structure due to an irradiation [10,22].

3.5. Comparison of the oxidation characteristics

Fig. 5 shows the temperature dependency of the oxidation rate of the as-received IG-11, IG-110 and IG-430 (here, the IG-11 was included for comparison with the IG-110 since the IG-11 is an un-purified version of IG-110 with a same recipe), and Fig. 6 compares the SEM photos of the oxidized surface at 1000 °C of the as-received and irradiated specimens. Fig. 7 compares the change of the pore area with the dose in the oxidized surfaces of the irradiated specimens.

In Fig. 5, while the differences in the oxidation rate between the purified IG-110 and IG-430 is small, and large differences are observed between the IG-11 and the other two purified nuclear grades, a higher oxidation rate of IG-110 than the IG-430 is observed through out the temperature ≫~800 °C. The observed higher oxidation rates in the IG-110 by TG in Fig. 5 can be confirmed in Fig. 6, where, both the as-received and lower dose condition (0.026 dpa) show a higher oxidation rate in the IG-110 than the IG-430. However, with an increase in the dose, the oxidation behaviors of the grades show a critical change, as observed in Figs. 6 and 7. Thus, for IG-110, the oxidation rate shows an apparent increase with a dose up to ~0.02 dpa (Fig. 7(a)). However, for a dose higher than ~0.02 dpa, the oxidation rate estimated by the changes in the pore area appears to decrease in IG-110. It is worth noting that the critical dose in Fig. 7, ~0.02 dpa, is similar to the critical dose in the (I_D/I_G)irr/$(I_D/I_G)_0$ – surface dose curve in Fig. 4(b) and (c), where, the (I_D/I_G)irr/$(I_D/I_G)_0$ shows a peak at ~0.02 dpa. This observation in both Figs. 7 and 4(b), 4(c) implies that a change in the irradiated microstructure has resulted in a pore area change. This observation may be attributed to an irradiation-induced defect formation and pore area reduction due to an amorphization [23,24].

In Fig. 7(a), contrary to the IG-110, the IG-430 shows a quite different oxidation behavior in that the pore area begins to decrease

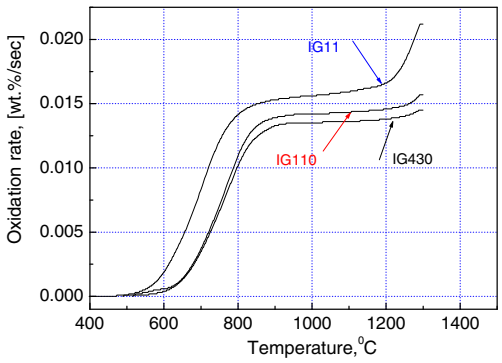

Fig. 5. The temperature dependency of the oxidation rate of the as-received, unirradiated IG-11, IG-110 and IG-430.

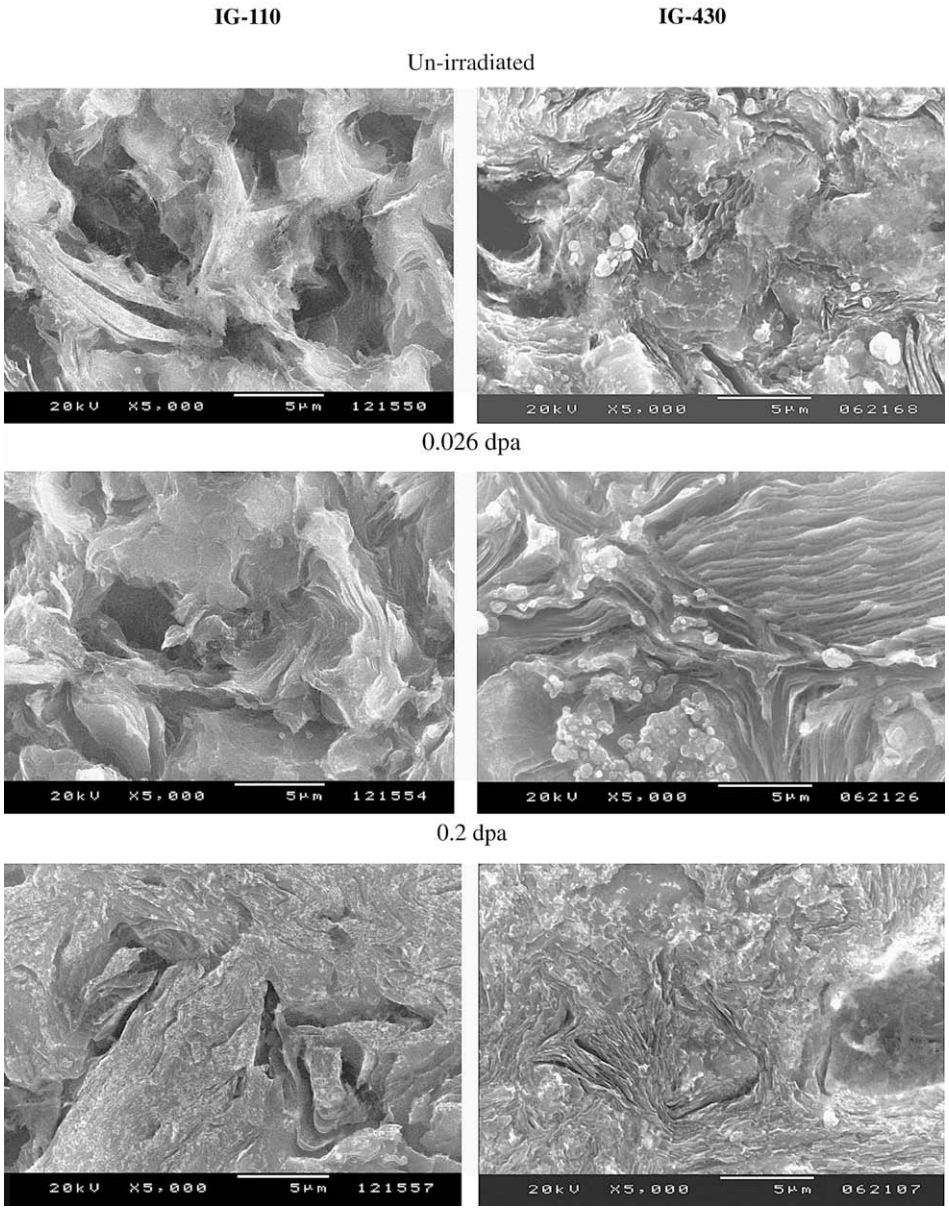

Fig. 6. Comparison of the oxidized surface (oxidized 30 min at 1000 °C before and after an irradiation).

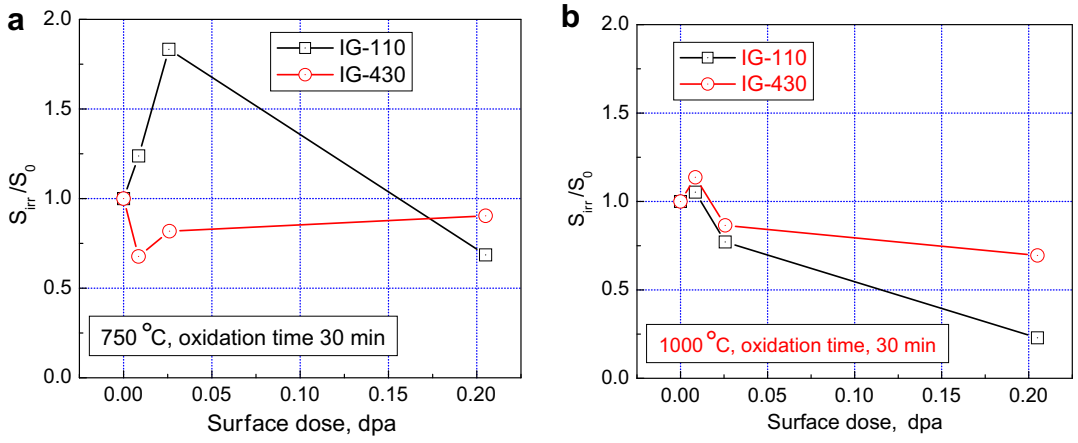

Fig. 7. The change of the pore area in the oxidized surfaces of irradiated specimens. Note the differences in the oxidation temperatures in Fig. 7: (a) 750 °C and (b) 1000 °C, respectively: S_0 – pore area on the oxidized surface of un-irradiated specimen. S_{irr} – pore area on the oxidized surface of irradiated specimen.

with the dose in the early stages of an irradiation, then, after a slight recovery in the oxidation rate, little changes are observed up to ~0.2 dpa. The reversal of the oxidation rate at ~0.17 dpa should be noted.

In Fig. 7(b) of the oxidation at 1000 °C, both grades show a continuous decrease in the pore area after a small increase by ~0.01 dpa, and, at ~0.2 dpa, the decrease in the pore area of the IG-110 is nearly three times that of IG-430. From the observation, a large dimensional change due to an irradiation may be assumed for IG-110 than the IG-430.

Apparent changes in the graphite microstructure due to an irradiation may be confirmed from the observation on the differences in the pore area due to an irradiation.

4. Discussion

4.1. Irradiation sensitivity

If the irradiation sensitivity of the grades is discussed in view of the degree of graphitization (DOG) and the as-received crystallinity, it is predicted that there will be no large differences in the irradiation sensitivity between the grades since the DOG and the FWHM of the grades are the same at 0.837 (Table 4), and as ~20 (Table 5).

Actually, as seen in Fig. 4(b) and (c), the overall results show little difference between the grades in the changes of the crystallinity and the crystallite size due to an irradiation. However, even the differences are not large, some small but apparent differences may be confirmed. Thus, the results of the oxidation and hardness test show a higher irradiation sensitivity for the IG-110, and the IG-430 shows a higher irradiation sensitivity in the crystallinity change estimated from the FWHM of the Raman spectrum of the D-peak. The changes in the crystallite size estimated from the intensity changes due to an irradiation, $(I_D/I_G)\mathrm{irr}/(I_D/I_G)_0$, show a larger decrease in IG-110.

The irradiation sensitivity of the grades appears to show a little change depending on the parameters evaluated. Of those parameters, the changes in the FWHM of the D-peak and the intensity of the Raman spectrum appear to show the highest sensitivity, Fig. 4(b) and (c). In Fig. 4(b) and (c), the higher development of the D-peak in the IG-430 than the IG-110 due to an irradiation may imply that the formation and the stabilization of the radiation-induced defects may be higher in the IG-430 than the IG-110. All these understandings and predictions may be attributed to the differences in the local graphite microstructure of the grades (thus, the degree of a graphitization). Here, it is worth to note the reversed responses of the crystallinity and crystallite size of the grades when analysed based on the results of Raman spectroscopy, Fig. 5. Thus, for the same dose, while a higher damage to crystallinity occurred in IG-430, a large decrease in the crystallite size was observed in IG-110. Further study will be required to understand the relationships between the changes in the microstructure and the Raman spectrum.

4.2. Oxidation

Oxidation experiment in the present study has resulted in three observations: (1) The oxidation rate of the IG-110 appeared higher than the IG-430 for both the un-irradiated and the irradiated conditions. (2) The oxidation rate of IG-110 increased with an increasing dose up to ~0.02 dpa, where the graphite begins an amorphization. (3) Amorphization resulted in a lower oxidation rate. To understand the present observation regarding (1), information on the fundamental differences between the grades on the factors that could have a strong influence on the obtained results needs to be compared. In this regards, some relevant information may be found from the TEM microscopy on the grades, Fig. 2, together with well proven relevant factors: density, porosity, and impurity.

As seen in Fig. 2 and Table 2, the large differences in the size and density of the Mrozowski cracks may also be considered as one of the key factors for the present observations in addition to the already well proven ones. It is easy to understand that a microstructure with a high density of large Mrozowski cracks will have more reaction sites for an oxidation.

Differences in the size and density of the Mrozowski cracks between the grades are attributed to the differences in the differential thermal strain of the crystallites of each grades [16].

The results of the lower oxidation rate of the amorphidized graphite can be understood partly from the decreasing pore area due to a volume contraction and an increase in the density with an increasing amorphization [23,24].

5. Conclusions

Comparisons made on the 3 MeV C^+ ion-irradiation effects on the microstructure (crystallinity, crystallite size), mechanical properties (hardness, Young's modulus), and oxidation properties of the IG-110 (petroleum coke) and IG-430 (coal tar pitch coke) showed, over all, a smaller or negligible differences between the grades. Large part of the observed similarity in the irradiation sensitivity between the grades may be attributed to the same degree of a graphitization (DOG) of the grades. However, even if the differences are not significant, some small but apparent differences were confirmed depending on the parameters examined. Thus, the results of the oxidation and hardness test showed higher irradiation sensitivity for the IG-110, and the IG-430 showed higher irradiation sensitivity for the crystallinity change. The changes in the crystallite size showed a larger decrease in IG-110. Of the parameters examined, the Raman spectra appeared to show the highest sensitivity to an irradiation. In particular, large sizes of the Mrozowski cracks in the IG-110 of a higher oxidation rate was noted.

Even if there are many limitations, a simulation of the neutron irradiation effects on nuclear graphite by an ion-irradiation may be useful, in particular, for the study of irradiation effects on the oxidation and the surface crystallinity (i.e., molecular bonding structure) of nuclear graphite.

Acknowledgements

The critical review and comments of Dr T. Burchell, ORNL, USA and helps from Drs W.S. Seo and Y.H. Lee, Korea Institute of Ceramic Engineering and Technology (KICET), for TEM are acknowledged. Concerns and supports from Drs Y.H. Kim, W.J. Lee, and J.H. Chang are appreciated. This work has been carried out as a part of Nuclear Hydrogen. Development and Demonstration project in Korea Atomic Energy Research Institute (KAERI) under the Nuclear R&D Program by Ministry of Education, Science and Technology (MEST), Korea.

References

[1] Collaboration Plan for Graphite Technology Development Area, PMB-VHTR/Materials and Components, GIV-International Forum, Rev. 0, June 2006.
[2] International Nuclear Graphite Specialist Meeting-7 Technical Program, ORNL, Oak Ridge, Tennessee, USA, 10–13 September 2006.
[3] ASTM E 521-96, Standard Practice for Neutron Radiation Damage Simulation by Charged-Particle Irradiation.
[4] W.P. Eatherly, E.L. Piper, Manufacture, in: R.E. Nightingale (Ed.), Nuclear Graphite, Academic Press, New York, 1962, p. 32.
[5] N. Iwashita, Chong Rae Park, H. Fujimoto, M. Shiraishi, M. Inagaki, Carbon 42 (2004) 701.

[6] F. Stevens, L.A. Kolodny, T.P. Beebe Jr., J. Phys. Chem. B 102 (1998) 10799.
[7] M. Doerner, W. Nix, J. Mater. Res. 1 (1986) 601.
[8] Se-Hwan Chi, Gen-Chan Kim, Jonghwa Chang, in: Proceedings of Second International Topical Meeting on High Temperature Reactor Technology, Beijing, China, 22–24 September 2004, #Paper F05.
[9] Gen-Chan Kim, Se-Hwan Chi, Jonghwa Chang, in: Proceedings of International Symposium of Chemical and Mechanical Polishing (ISCMP-2005), 27 August 2005, Cheongju, p. 75.
[10] Se-Hwan Chi, Gen-Chan Kim, et al., Mater. Sci. Forum 475–470 (2005) 1471.
[11] W. Oliver, G. Pharr, J. Mater. Res. 7 (1992) 1564.
[12] A.C. Ferrari, J. Robertson, Phys. Rev. B 61 (20) (2000) 14095.
[13] F. Tuinstra, J.L. Koenig, J. Chem. Phys. 53 (3) (1970) 1126.
[14] K. Nakamura, M. Kitajima, Phys. Rev. B 45 (1992) 78.
[15] Se-Hwan Chi, Gen-Chan Kim, et al., in: Proceedings of ICAPP 2005, Seoul, Korea, 15–19 May 2005.
[16] J.L. White, in: J.O. McCaldin, G. Somorjal (Eds.), Progress in Solid State Chemistry, vol. 9, Pergamon, Oxford, 1975, p. 91.
[17] G. Katagiri, Tanso 175 (1996) 304–313 (in Japanese).
[18] K. Niwase, Phys. Rev. B 52 (1995) 15785.
[19] Gen-Chan Kim, Se-Hwan Chi, Jong-Hwa Chang, in: Proceedings of Korea Nuclear Society Fall Meeting, Busan, Korea, 28–29 October 2005.
[20] T. Tanabe, T. Maruyama, M. Iseki, K. Niwase, H. Atsumi, Fusion Eng. Design 29 (1995) 428.
[21] K. Niwase, K. Nakamura, et al., J. Nucl. Mater. 170 (1990) 106.
[22] Se-Hwan Chi, Gen-Chan Kim, et al., in: Proceedings of the Fourth International Nuclear Graphite Specialist Meeting, Marugame, Japan, 13–16 September 2003.
[23] K. Niwase, Philos. Mag. Lett. 82 (2002) 401.
[24] D.G. McCulloch, A. Hoffman, S. Prawer, J. Appl. Phys. 74 (1993) 135.